Hindawi
International Journal of Aerospace Engineering
Volume 2022, Article ID 9931498, 14 pages
https://doi.org/10.1155/2022/9931498

Research Article

Quasi-One-Dimensional Model of Hydrocarbon-Fueled Scramjet Combustor Coupled with Regenerative Cooling

Yuefei Xiong,[1] Jiang Qin,[1] Kunlin Cheng,[1] Silong Zhang,[1] and Yu Feng[2]

[1]*School of Energy Science and Engineering, Harbin Institute of Technology, Harbin 150001, China*
[2]*Department of Mechanical Engineering and Automation, Harbin Institute of Technology (Shenzhen), Shenzhen 518055, China*

Correspondence should be addressed to Jiang Qin; qinjiang@hit.edu.cn

Received 14 April 2022; Revised 28 June 2022; Accepted 8 July 2022; Published 8 August 2022

Academic Editor: Shunan Wu

In order to rapidly predict the performance of hydrocarbon-fueled regeneratively cooled scramjet engine in system design, a quasi-one-dimensional model has been developed. The model consists of a supersonic combustor model with finite-rate chemistry and a cooling channel model with real gas working medium, which are governed by two sets of ordinary differential equations separately. Additional models for wall friction, heat transfer, sonic fuel injection, and mixing efficiency are also included. The two sets of ordinary differential equations are coupled and iteratively solved. The SUNDIALS code is used since the equations for supersonic combustion flow are stiff mathematically. The cooling channel model was verified by electric heating tube tests, and the supersonic combustor model was verified by experimental results for both hydrogen and hydrocarbon-fueled scramjet combustors. Three cases were comparatively studied: (1) scramjet combustor with an isothermal wall, (2) scramjet combustor with an adiabatic wall, and (3) scramjet combustor with regenerative cooling. Results showed that the model could predict the axial distributions of flow parameters in the supersonic combustor and cooling channel. Differences on ignition delay time and combustion efficiency for the three cases were observed.

1. Introduction

Scramjet engines are regarded as the next-generation propulsion engine for air-breathing vehicles [1–3]. The biggest difference between scramjet engines and traditional ones is that the combustion process of scramjet engines is taken place in supersonic flow which makes scramjet engines to be operated at hypersonic speeds. Compared with traditional air-breathing engines such as turbine jet engines and ramjet engines, the flight speeds of scramjet engines are much faster. Theoretically scramjet engines can be operated at Mach numbers above 10 [4]. As air-breathing engines, the fuel impulses of scramjet engines are much higher than the one of rocket engines. So scramjet engines are suitable for high-speed and long-duration flights. Although scramjet engines cannot be operated at low speeds, combined systems composed of scramjet engines such as RBCC (Rocket-Based Combined Cycle) [5] and TBCC (Turbine-Based Combined Cycle) [6] can take off at the zero speed. Because of these performance advantages, scramjet engines have attracted more and more attentions. After decades of research, scramjet engine technology becomes more mature. Its viability has been demonstrated by the past flight tests [7, 8], based on which the actual application of scramjet engines is increasingly possible.

In the early design of scramjet engines, it is important to predict the engine performance accurately and efficiently. Multidimensional numerical simulation by supercomputers can get a relatively accurate performance prediction of scramjet engines. However, it costs a lot of computing resources and time. Compared with multidimensional numerical simulation, the quasi-one-dimensional calculation is much more efficient. And the computational accuracy is acceptable. So the quasi-one-dimensional calculation is widely adopted in the performance prediction of scramjet engines. And the quasi-one-dimensional model plays an important role.

Various quasi-one-dimensional models of scramjet engines with different assumptions have been put forward. Tsujikawa et al. [9] proposed a quasi-one-dimensional

model for the scramjet engine based on which the engine performance was analyzed and the engine configuration was optimized. For the combustion reaction, a global hydrogen-air combustion model with a two-step reaction mechanism was adopted. O'Brien et al. [10] developed a quasi-one-dimensional scramjet combustor model with finite-rate chemistry. The fuel ignition position was accurately predicted by the model as well as the wall pressure profiles. Tetlow and Doolan [11] comparatively studied the performance of hydrogen and hydrocarbon-fueled scramjet engine for orbital insertion based on a quasi-one-dimensional model. Results showed that the hydrogen-fuel scramjet engine outperformed the hydrocarbon-fueled scramjet engine due to its higher specific impulse and peak Mach number. Tomioka et al. [12] conducted quasi-one-dimensional analyses with both chemical equilibrium and finite-rate reaction to investigate the vitiation effects on scramjet engine performance in Mach 6 flight conditions. Brizer and Doolan [13] produced a quasi-one-dimensional model of hydrogen-fuel scramjet combustor with the assumption that the combustion was a mixing-controlled process, based on which the computational efficiency was further improved. Kang et al. [14] investigated the effects of flame holder configurations on the combustion of a scramjet combustor through experiments, numerical simulations, and quasi-one-dimensional analyses. Noda et al. [15] carried out a quasi-one-dimensional calculation to study the performance of a supersonic combustor. Experimental results showed that the calculated results had a reasonable accuracy. The mode-transition equivalence ratio and the thrust performance of the supersonic combustor were also investigated based on the quasi-one-dimensional model. Bao et al. [16] developed a quasi-one-dimensional model for a hydrogen-fueled regeneratively cooled scramjet combustor using MacCormack's method. Based on the model, the influence of the cooling channel geometry, flight Mach number, and fuel equivalence ratio on the performance of the regenerative cooling system was investigated. Tian et al. [17] proposed a quasi-one-dimensional analytical method with a novel model for pre-combustion shock train, based on which different modes of a dual-mode scramjet combustor were analyzed. The effect of heat release distribution and engine structure on the net thrust of the scramjet engine was also investigated [18]. Results showed that the analytical method could be used for the optimization of high-performance scramjet engines. Goel et al. [19] adopted retrospective cost adaptive control to control the thrust of the scramjet engine based on a quasi-one-dimensional model. Wang et al. [20] established a quasi-one-dimensional numerical method to simplify the unsteady combustion and flow of the solid-fuel scramjet engine. Results predicted by the model were in good agreement with the experimental data. Based on the model, the parametric changing process of the combustor was calculated quickly. Smart [21] developed a quasi-one-dimensional analysis technique to calculate the flow through a pseudoshock. Results indicated that the technique could predict accurately both the interaction length and the pressure distribution for X-type pseudoshocks with Mach numbers above two. Vanyai et al. [22] developed a novel quasi-one-dimensional model for scramjet combustors in which the combustion process was predetermined. Four ideal combustion processes occurred in the scramjet combustor, which were comparatively analyzed. Results showed that engines with a combination of different combustion processes had the best performance. Cheng et al. [23] developed a quasi-one-dimensional expansion model coupled with wall cooling to analyze the expansion process of scramjet engines with recuperation. Results showed that the recuperation process by wall cooling in the nozzle could improve the performance of the scramjet engine. Schetz et al. [24] developed a quasi-one-dimensional model to conduct the analysis of slot injection in hypersonic flow. Based on the model, Kanda et al. [25] studied the effect of film cooling/regenerative cooling on scramjet engine performance. Zuo et al. [26] further investigated the cooling effect of the combined cooling technique. Results showed that the combined cooling technique had a good effect on reducing the engine wall temperature; meanwhile, the flight Mach number could be increased by nearly 8%.

For the scramjet engine designed for long-range flight, regenerative cooling is usually employed [27]. Zhang et al. [28] developed a quasi-one-dimensional model of a scramjet combustor coupled with regenerative cooling. Hydrogen was chosen as fuel in the model. Differences on mixing efficiency, ignition delay time, heat flux, and engine performance were observed in his study.

Zhang's work is remarkable and meaningful. However, hydrocarbon fuels are better fuel candidates than hydrogen for scramjet engines. The density of a hydrocarbon is much higher than the one of hydrogen, which means the volume of a fuel tank of hydrocarbons is much smaller than the one of hydrogen. Vehicles powered by hydrocarbon-fueled scramjet engines own less weight and drag. Hydrocarbon fuels have the largest possibility to be fuel of scramjet engines, and the research tendency has proven it. The vehicle X-43 A adopts hydrogen as fuel [29, 30], but the successor X-51 A uses hydrocarbon fuel as fuel [31]. So a quasi-one-dimensional model of hydrocarbon-fueled scramjet combustors coupled with regenerative cooling is necessary and important. Such a model is developed in this work, based on which the characteristics of a hydrocarbon-fueled regeneratively cooled scramjet combustor are analyzed.

2. Model of the Supersonic Combustor

The supersonic combustor model is composed of a set of ordinary differential equations. By solving the equations, flow variables in the combustor for certain inlet conditions and fuel equivalence ratios can be obtained. Models of mixing, heat transfer, and wall friction are also provided. The mixing process of fuel and air along the combustor duct is represented by adopting the concept of mixing efficiency. The amount of heat transferred through the combustor wall and the wall friction coefficient can be calculated by using Eckert's reference enthalpy method.

2.1. Governing Equations. The supersonic combustor model is based on the following assumptions:

(1) The flow is quasi-one-dimensional, and all flow variables and the cross-sectional area of the combustor duct are functions of the axial distance x along the duct

(2) The flow is steady-state

(3) The flow is regarded as a perfect gas

The continuity equation of a steady-state flow can be expressed in differential form as

$$\frac{1}{\dot{m}}\frac{d\dot{m}}{dx} = \frac{1}{\rho}\frac{d\rho}{dx} + \frac{1}{U}\frac{dU}{dx} + \frac{1}{A_{\text{comb}}}\frac{dA_{\text{comb}}}{dx}. \quad (1)$$

Variation in mass injection $d\dot{m}/dx$ of fuel and cross-sectional area dA_{comb}/dx of the combustor duct can be got by providing a mass injection rate and an area profile.

Considering fuel injection and wall friction, the momentum equation in differential form can be expressed as

$$\frac{1}{p}\frac{dp}{dx} + \frac{\gamma Ma^2}{U}\frac{dU}{dx} + \frac{2\gamma Ma^2 C_f}{D} + \frac{\gamma Ma^2(1-\varepsilon)}{\dot{m}}\frac{d\dot{m}}{dx} = 0, \quad (2)$$

where γ is the specific heat ratio, C_f is the wall friction coefficient, D is the hydraulic diameter of the combustor duct, and ε is the ratio of fuel injection velocity in x direction to main flow velocity.

Since the temperature in the combustor is very high, the main flow behaves as a perfect gas. The differential form of the equation of state (EoS) can be expressed as

$$\frac{1}{p}\frac{dp}{dx} = \frac{1}{\rho}\frac{d\rho}{dx} + \frac{1}{T}\frac{dT}{dx} - \frac{1}{\overline{M_w}}\frac{d\overline{M_w}}{dx}. \quad (3)$$

The mixture molecular weight $\overline{M_w}$ can be expressed in terms of the mass friction as

$$\overline{M_w} = \frac{1}{\sum_i y_i/M_{w,i}}. \quad (4)$$

Expressing the mixture molecular weight $\overline{M_w}$ in differential form yields

$$\frac{d\overline{M_w}}{dx} = -\overline{M_w}^2\left(\sum_i \frac{1}{M_{w,i}}\frac{dy_i}{dx}\right). \quad (5)$$

The mass or mole friction of species can be changed by fuel injection and chemical reaction. The differential form of the species conservation equation can be expressed as

$$\frac{dy_i}{dx} = \frac{\dot{\omega}_i M_{w,i}}{\rho U} + \frac{1}{\dot{m}}\frac{d\dot{m}_{i,added}}{dx} - \frac{y_i}{\dot{m}}\frac{d\dot{m}}{dx}, \quad (6)$$

where $\dot{\omega}_i$ is the chemical production rate of species i and $\dot{m}_{i,\text{added}}$ is the mass addition of species i. The first term on the right-hand side of equation (6) represents the mass friction change caused by chemical reaction. Fuel injection can cause the increase in mass friction of some species and the decrease in mass friction of other species because of the dilution effect, which are represented in the second and third term, respectively.

By neglecting axial heat conduction, axial species diffusion, and thermal radiation, the differential form of the energy equation can be expressed as

$$\frac{dh}{dx} = \frac{1}{\dot{m}}\frac{d\sum_i (h_{o,i}\dot{m}_i)_{\text{added}}}{dx} - \frac{q_w P_w}{\dot{m}} - \frac{h_o}{\dot{m}}\frac{d\dot{m}}{dx} - U\frac{dU}{dx}, \quad (7)$$

where

$$h_o = h + \frac{1}{2}U^2, \quad (8)$$

$$\frac{dh}{dx} = \sum_i h_i\frac{dy_i}{dx} + c_p\frac{dT}{dx}. \quad (9)$$

In equation (7), the term $d\sum_i (h_{o,i}\dot{m}_i)_{\text{added}}$ represents total enthalpy increased by fuel injection, and the term $q_w P_w dx$ means heat loss through the combustor wall.

Combining equation (1)–(9) gives the complete set of ordinary differential equations for the supersonic combustor model.

$$\frac{dy_i}{dx} = \frac{\dot{\omega}_i M_{w,i}}{\rho U} + \frac{1}{\dot{m}}\frac{d\dot{m}_{i,\text{added}}}{dx} - \frac{y_i}{\dot{m}}\frac{d\dot{m}}{dx}, \quad (10)$$

$$\frac{d\overline{M_w}}{dx} = -\overline{M_w}^2\left(\sum_i \frac{1}{M_{w,i}}\frac{dy_i}{dx}\right), \quad (11)$$

$$\frac{d\rho}{dx} = \rho\left[\frac{1}{\dot{m}}\frac{d\dot{m}}{dx} - \frac{1}{U}\frac{dU}{dx} - \frac{1}{A_{\text{comb}}}\frac{dA_{\text{comb}}}{dx}\right], \quad (12)$$

$$\frac{dp}{dx} = -\frac{pU^2\overline{M_w}}{R_u T}\left[\frac{1}{U}\frac{dU}{dx} + \frac{2C_f}{D} + \frac{(1-\varepsilon)}{\dot{m}}\frac{d\dot{m}}{dx}\right], \quad (13)$$

$$\begin{aligned}\frac{dU}{dx} = \frac{1}{\alpha}\Bigg\{&-\frac{1}{A_{\text{comb}}}\frac{dA_{\text{comb}}}{dx} + \frac{1+\gamma M^2(1-\varepsilon) - h_o/(Tc_p)}{\dot{m}}\frac{d\dot{m}}{dx} \\ &+ \frac{1}{Tc_p}\left[-\sum_i h_i\frac{dy_i}{dx} + \frac{1}{\dot{m}}\sum_i\left(h_{o,i,\text{added}}\frac{d\dot{m}_{i,\text{added}}}{dx}\right)\right] \\ &- \frac{1}{\overline{M_w}}\frac{d\overline{M_w}}{dx} + \frac{2C_f U^2\overline{M_w}}{R_u TD} - \frac{q_w P_w}{Tc_p\dot{m}}\Bigg\},\end{aligned} \quad (14)$$

$$\frac{dT}{dx} = T\left[\frac{1}{p}\frac{dp}{dx} - \frac{1}{\rho}\frac{d\rho}{dx} + \frac{1}{\overline{M_w}}\frac{d\overline{M_w}}{dx}\right], \quad (15)$$

$$\alpha = \frac{1}{U} - \frac{U\overline{M_w}}{R_u T} + \frac{U}{Tc_p}, \quad (16)$$

$$h_o = h + \frac{1}{2}U^2. \quad (17)$$

In order to calculate the chemical production rates of species, a simplified reaction mechanism including 34 steps

with 24 species based on the mechanism proposed by Kundu et al. [32] is used in this study.

2.2. Supersonic Mixing. In order to accurately predict the performance of a scramjet engine, a reasonable assumption of heat release distribution along the combustor duct is crucial, which is performed by deriving a supersonic mixing model. In the current model, the concept of mixing efficiency is adopted to determine the fuel flow rate available for combustion.

$$\dot{m}_{fc} = \eta_m \dot{m}_f, \tag{18}$$

where $\dot{m}_{fc}$ is the mass flow rate of fuel available for combustion and $\dot{m}_f$ is the mass flow rate of fuel injected into the combustor. The mixing efficiency η_m changes from zero at the location of fuel injector to unity at a defined mixing length L_{mix}. The mixing efficiency η_m and the mixing length L_{mix} can be calculated by the following equations [13].

$$\text{Ma}_c = \frac{U_f - U_a}{a_f + a_a}, \tag{19}$$

$$f(\text{Ma}_c) = 0.25 + 0.75 \exp\left(-3\text{Ma}_c^2\right), \tag{20}$$

$$\left(\frac{L_{\text{mix}}}{d_f}\right) = \frac{K}{f(\text{Ma}_c)} \left(\frac{\rho_f U_f}{\rho_a U_a}\right)^{0.5}, \tag{21}$$

$$\eta_m = b\left(1 - \exp\left(-(c\bar{x})^d\right)\right), \tag{22}$$

$$\bar{x} = \frac{x - L_{\text{inj}}}{L_{\text{mix}}}, \tag{23}$$

where U_f, a_f, and ρ_f are velocity, sound speed, and density of fuel at the outlet of the fuel injector which can be obtained by the model of the fuel injector, respectively. Variables U_a, a_a, and ρ_a are velocity, sound speed, and density of the main flow at the location of the fuel injector, respectively. According to [13], values of constants in equation (22) are as follows: $b = 1.06492$, $c = 3.69639$, and $d = 0.80586$. The value of constant K for strut-injected scramjet engines is 390. The fuel flow rate available for combustion can be obtained by the above mixing model.

2.3. Calculation of the Heat Flux and the Wall Frication Coefficient. Accurate calculation of the heat flux through the combustor wall is important because it can simultaneously affect the flow parameters in the combustor and cooling channel. Eckert's reference enthalpy method [4] is adopted in this study. The density of heat flux through the combustor wall and the wall friction coefficient can be calculated by the following equations.

$$h^* = \frac{h + h_w}{2} + 0.22r\frac{U^2}{2}, \tag{24}$$

$$\text{r} = \sqrt[3]{\text{Pr}^*} = \sqrt[3]{\frac{\mu^* c_p^*}{\lambda^*}}, \tag{25}$$

$$q_w = \frac{0.0287 p U \overline{M_w}(h_{aw} - h_w)}{R_u T^* \text{Pr}^{*0.4} \text{Re}_x^{*0.2}}, \tag{26}$$

$$h_{aw} = h + \frac{U^2}{2}, \tag{27}$$

$$\text{Re}_x^* = \frac{p U \overline{M_w} x}{R_u T^* \mu^*}, \tag{28}$$

$$C_f = \frac{0.0574}{\text{Re}_x^{*0.2}} \frac{T}{T^*}, \tag{29}$$

where the variables with superscript $*$ are calculated with the reference temperature T^*. The reference temperature T^* can be obtained by iterative calculation from equations (24) and (25).

3. Model of the Cooling Channel and the Fuel Injector

The model of the cooling channel is similar to the one of the supersonic combustor, except for the complexity caused by the thermodynamic properties of real gases. Since the flow in the cooling channel is subsonic, the flow variables in the cooling channel are solved together with the fuel injector to offer boundary conditions for the supersonic combustor. For simplicity, an isentropic sonic fuel injector is used in this study.

3.1. Thermodynamic Property Calculation of a Multicomponent Mixture

3.1.1. Density Calculation of a Multicomponent Mixture. In this study, the RK-PR equation is chosen as the EoS (Equation of State) of real gases. Since the cracking products of fuel contain a lot of species, the EoS must be extended to satisfy the density calculation of a multicomponent mixture. Here, by assuming the multicomponent mixture to be a single-component gas, its density can be calculated by the following mixing rules [33]:

$$a\alpha = \sum_{i=1}^{N} \sum_{j=1}^{N} x_i x_j a_{ij} \alpha_{ij}, \tag{30}$$

$$b = \sum_{i=1}^{N} x_i b_i, \tag{31}$$

$$\delta_1 = \sum_{i=1}^{N} x_i \delta_{1,i}, \tag{32}$$

$$\delta_2 = \frac{1 - \delta_1}{1 + \delta_1}, \tag{33}$$

$$a_{ij}\alpha_{ij} = \sqrt{a_i a_j \alpha_i \alpha_j}\left(1 - \kappa_{ij}\right), \tag{34}$$

where κ_{ij} is an empirical parameter of binary interaction between species i and j. For hydrocarbons, it takes a value of

0. For a mixture containing hydrogen, it needs to change the value of the critical compressibility factor of hydrogen to 0.2897 in the calculation of δ_{1,H_2}, or no real solution will be got [34].

3.1.2. Thermodynamic Property Calculation Based on the EoS. The thermodynamic properties of a real gas can be obtained by modifying the corresponding values of an ideal gas. Here, the modification is accomplished by applying the general relations of thermodynamic properties of real gases [35]. The final mathematic formulas of thermodynamic properties of a real gas are listed as follows:

$$e_m = e_{m,0} + \frac{1}{(\delta_1 - \delta_2) b M_w}\left[T\left(\frac{\partial a\alpha}{\partial T}\right) - a\alpha\right] \ln\left(\frac{M_w + \delta_1 b\rho}{M_w + \delta_2 b\rho}\right), \tag{35}$$

$$h_m = e_m + \frac{p}{\rho}, \tag{36}$$

$$c_{v,m} = c_{v,m,0} + \frac{T}{(\delta_1 - \delta_2) b M_w}\left(\frac{\partial^2 a\alpha}{\partial T^2}\right) \ln\left(\frac{M_w + \delta_1 b\rho}{M_w + \delta_2 b\rho}\right), \tag{37}$$

$$c_{p,m} = c_{v,m} + \frac{T}{\rho^2}\left\{\frac{\left[(\rho R_u/(M_w - b\rho)) - (\partial a\alpha/\partial T)\left(\rho^2/(M_w + \delta_1 b\rho)(M_w + \delta_2 b\rho)\right)\right]^2}{\left(M_w R_u T/(M_w - b\rho)^2\right) - \left(a\alpha\rho M_w[2M_w + (\delta_1 + \delta_2)b\rho]/(M_w + \delta_1 b\rho)^2(M_w + \delta_2 b\rho)^2\right)}\right\}, \tag{38}$$

$$\gamma_m = \frac{c_{p,m}}{c_{v,m}}, \tag{39}$$

$$s_m = s_{m,0} + \frac{R_u}{M_w} \ln\left(1 - \frac{b\rho}{M_w}\right) - \frac{R_u}{M_w} \ln\left(\frac{\rho}{\rho_0}\right) + \left(\frac{\partial a\alpha}{\partial T}\right) \frac{1}{(\delta_1 - \delta_2) b M_w} \ln\left(\frac{M_w + \delta_1 b\rho}{M_w + \delta_2 b\rho}\right), \tag{40}$$

$$s_{m,0} = \sum_{i=1}^{N}\left[s^{\circ}_{0,i} - \frac{R_u}{M_{w,i}} \ln\left(\frac{x_i p}{p^{\circ}}\right)\right] y_i. \tag{41}$$

3.2. Governing Equations for the Cooling Channel. The model of the cooling channel is based on the following assumptions:

(1) The flow is quasi-one-dimensional, and all flow variables and the cross-sectional area of the cooling channel are functions of the axial distance x along the duct

(2) The flow is steady-state

(3) The flow is a reacting flow

(4) The working medium is regarded as a real gas

The differential form of the continuity equation is shown as follows:

$$\frac{1}{\rho}\frac{d\rho}{dx} + \frac{1}{U}\frac{dU}{dx} + \frac{1}{A_c}\frac{dA_c}{dx} = 0. \tag{42}$$

The momentum equation can be expressed in differential form as

$$\dot{m}_f \frac{dU}{dx} + A_c \frac{dp}{dx} + \frac{1}{2}\frac{f}{D_r}\dot{m}_f U = 0, \tag{43}$$

where f is the drag coefficient of the cooling channel which can be predicted by the Colebrook method shown in

$$\frac{1}{\sqrt{f}} = -2\lg\left(\frac{\Delta/D_r}{3.7} + \frac{2.51}{\mathrm{Re}\sqrt{f}}\right). \tag{44}$$

In the cooling channel, fuel behaves as a real gas whose state is described by the RK-PR equation in this study. The EoS in differential form can be expressed as

$$\begin{aligned}\frac{dp}{dx} = \bar{A}\frac{d\rho}{dx} + \bar{B}\frac{dT}{dx} + \bar{C}\frac{d\overline{M_{wf}}}{dx} + \bar{D}\sum_{i=1}^{N} b_i \frac{dx_i}{dx} \\ + \bar{E}\sum_{i=1}^{N}\sqrt{a_i\alpha_i}\frac{dx_i}{dx} + \bar{F}\sum_{i=1}^{N}\delta_{1,i}\frac{dx_i}{dx},\end{aligned} \tag{45}$$

where

$$\bar{A} = \frac{R_u T \overline{M_{wf}}}{\left(\overline{M_{wf}} - b\rho\right)^2} - \frac{2a\alpha\rho\overline{M_{wf}}^2 + (\delta_1 + \delta_2)a\alpha b\rho^2\overline{M_{wf}}}{\left(\overline{M_{wf}} + \delta_1 b\rho\right)^2\left(\overline{M_{wf}} + \delta_2 b\rho\right)^2}, \tag{46}$$

$$\bar{B} = \frac{R_u \rho}{\overline{M_{wf}} - b\rho} - \frac{\sqrt{a\alpha}\rho^2}{\left(\overline{M_{wf}} + \delta_1 b\rho\right)\left(\overline{M_{wf}} + \delta_2 b\rho\right)} \sum_{i=1}^{N} \frac{\sqrt{a_i}x_i}{\sqrt{\alpha_i}} \frac{\partial \alpha_i}{\partial T}, \quad (47)$$

$$\bar{C} = \frac{2a\alpha\rho^2\overline{M_{wf}} + (\delta_1 + \delta_2)a\alpha b\rho^3}{\left(\overline{M_{wf}} + \delta_1 b\rho\right)^2\left(\overline{M_{wf}} + \delta_2 b\rho\right)^2} - \frac{\rho R_u T}{\left(\overline{M_{wf}} - b\rho\right)^2}, \quad (48)$$

$$\bar{D} = \frac{\rho^2 R_u T}{\left(\overline{M_{wf}} - b\rho\right)^2} + \frac{(\delta_1 + \delta_2)a\alpha\rho^3\overline{M_{wf}} + 2\delta_1\delta_2 a\alpha b\rho^4}{\left(\overline{M_{wf}} + \delta_1 b\rho\right)^2\left(\overline{M_{wf}} + \delta_2 b\rho\right)^2}, \quad (49)$$

$$\bar{E} = \frac{-2\sqrt{a\alpha}\rho^2}{\left(\overline{M_{wf}} + \delta_1 b\rho\right)\left(\overline{M_{wf}} + \delta_2 b\rho\right)}, \quad (50)$$

$$\bar{F} = \frac{a\alpha b\rho^3\left[\left(\overline{M_{wf}} + \delta_2 b\rho\right) - 2\left(\overline{M_{wf}} + \delta_1 b\rho\right)/(1+\delta_1)^2\right]}{\left(\overline{M_{wf}} + \delta_1 b\rho\right)^2\left(\overline{M_{wf}} + \delta_2 b\rho\right)^2}, \quad (51)$$

$$\frac{dx_i}{dx} = \frac{\overline{M_{wf}}}{M_{w,i}}\frac{dy_i}{dx} + \frac{y_i}{M_{w,i}}\frac{d\overline{M_{wf}}}{dx}. \quad (52)$$

The differential form of the mixture molecular weight $\overline{M_{wf}}$ can be expressed as

$$\frac{d\overline{M_{wf}}}{dx} = -\overline{M_{wf}}^2\left(\sum_i \frac{1}{M_{w,i}}\frac{dy_i}{dx}\right). \quad (53)$$

The differential form of the species conversation equation can be expressed as

$$\frac{dy_i}{dx} = \frac{\dot{\omega}_i M_{w,i} A_c}{\dot{m}_f}, \quad (54)$$

where $\dot{\omega}_i$ is the chemical production rate of species i.

The differential form of the energy equation is shown in equation (55). The three terms of the right-hand side of equation (55) represent the influence of temperature, pressure, and species on the enthalpy of mixture, respectively.

$$\frac{dh}{dx} = B_T\frac{dT}{dx} + B_p\frac{dp}{dx} + \sum_{i=1}^{N-1} B_{y_i}\frac{dy_i}{dx}, \quad (55)$$

where

$$B_T = c_{v,m} + \frac{T}{\rho^2}\left(\frac{\left(\partial p/\partial T\right)^2_{\rho_i}}{\left(\partial p/\partial\rho\right)_{T,y_i}}\right) = c_{p,m}, \quad (56)$$

$$B_p = \frac{1}{\rho} - \frac{T}{\rho^2}\left(\frac{\left(\partial p/\partial T\right)_{\rho_i}}{\left(\partial p/\partial\rho\right)_{T,y_i}}\right), \quad (57)$$

$$B_{y_i} = \left(\tilde{e}_i - \tilde{e}_N\right) + \frac{T}{\rho}\left[\left(\frac{\partial p}{\partial \rho_i}\right)_{T,\rho_{j\neq i}} - \left(\frac{\partial p}{\partial \rho_N}\right)_{T,\rho_{j\neq N}}\right]\frac{\left(\partial p/\partial T\right)_{\rho_i}}{\left(\partial p/\partial\rho\right)_{T,y_i}}, \quad (58)$$

$$\begin{aligned}\tilde{e}_i = \left(\frac{\partial \rho e}{\partial \rho_i}\right)_{T,\rho_{j\neq i}} &= e_{0,i} + \frac{2}{(\delta_1 - \delta_2)bM_{w,i}} \\ &\cdot \left[\sum_j x_j\left(T\frac{\partial\left(a_{ij}\alpha_{ij}\right)}{\partial T} - a_{ij}\alpha_{ij}\right)\right]\ln\left(\frac{\overline{M_{wf}} + \delta_1 b\rho}{\overline{M_{wf}} + \delta_2 b\rho}\right) \\ &+ \frac{bi}{(\delta_1 - \delta_2)bM_{w,i}}\left[T\frac{\partial(a\alpha)}{\partial T} - a\alpha\right] \\ &\cdot \left[\frac{(\delta_1 - \delta_2)\rho\overline{M_{wf}}}{\left(\overline{M_{wf}} + \delta_1 b\rho\right)\left(\overline{M_{wf}} + \delta_2 b\rho\right)} - \frac{1}{b}\ln\left(\frac{\overline{M_{wf}} + \delta_1 b\rho}{\overline{M_{wf}} + \delta_2 b\rho}\right)\right],\end{aligned} \quad (59)$$

$$\begin{aligned}\left(\frac{\partial p}{\partial \rho_i}\right)_{T,\rho_{j\neq i}} &= \frac{\overline{M_{wf}}R_u T}{M_{w,i}\left(\overline{M_{wf}} - b\rho\right)^2}\left[\overline{M_{wf}} + \rho(b_i - b)\right] \\ &- \frac{2\rho\overline{M_{wf}}\sum_j x_j a_{ij}\alpha_{ij}}{M_{w,i}\left(\overline{M_{wf}} + \delta_1 b\rho\right)\left(\overline{M_{wf}} + \delta_2 b\rho\right)} \\ &+ \frac{a\alpha\rho^2\overline{M_{wf}}D_d}{M_{w,i}(1+\delta_1)\left(\overline{M_{wf}} + \delta_1 b\rho\right)^2\left(\overline{M_{wf}} + \delta_2 b\rho\right)^2},\end{aligned} \quad (60)$$

$$\begin{aligned}D_d = \rho\left[b^2\delta_{1,i}(\delta_2 - \delta_1) + 2b\delta_1\delta_2 b_i(1+\delta_1) - b^2\delta_1(\delta_2 - \delta_1)\right] \\ + \overline{M_{wf}}\left[-b\delta_{1,i}(\delta_2 - \delta_1) + (1+\delta_1)(\delta_2 + \delta_1)b_i + b\delta_1(\delta_2 - \delta_1)\right].\end{aligned} \quad (61)$$

The complete set of ordinary differential equations for the cooling channel model is shown as follows:

$$\frac{dy_i}{dx} = \frac{\dot{\omega}_i M_{w,i} A_c}{\dot{m}_f}, \quad (62)$$

$$\frac{d\overline{M_{wf}}}{dx} = -\overline{M_{wf}}^2\left(\sum_i \frac{1}{M_{w,i}}\frac{dy_i}{dx}\right), \quad (63)$$

$$\frac{dU}{dx} = \frac{\left[\left(f\dot{m}_f U\left(B_T + \bar{B}B_p\right)/2D_r A_c B_T\right) - \left(\bar{A}\rho/A_c\right)\left(dA_c/dx\right) + \bar{C}\left(d\overline{M_{wf}}/dx\right) + \bar{D}\sum_{i=1}^{N} b_i\left(dx_i/dx\right) + \bar{E}\sum_{i=1}^{N}\sqrt{a_i\alpha_i}\left(dx_i/dx\right) + \bar{F}\sum_{i=1}^{N}\delta_{1,i}\left(dx_i/dx\right) + \left(\bar{B}q_w P_w/B_T\dot{m}_f\right) - \left(\bar{B}/B_T\right)\sum_{i=1}^{N-1} B_{y_i}\left(dy_i/dx\right)\right]}{\left[\left(\bar{B}U/B_T\right) + \left(\bar{A}\rho/U\right) - \left(\left(B_T + \bar{B}B_p\right)\dot{m}_f/B_T A_c\right)\right]}, \quad (64)$$

$$\frac{dp}{dx} = -\frac{f\dot{m}_f U}{2D_r A_c} - \frac{\dot{m}_f}{A_c}\frac{dU}{dx}, \quad (65)$$

$$\frac{d\rho}{dx} = -\frac{\rho}{U}\frac{dU}{dx} - \frac{\rho}{A_c}\frac{dA_c}{dx}, \quad (66)$$

$$\frac{dT}{dx} = \frac{q_w P_w}{B_T\dot{m}_f} - \frac{B_p}{B_T}\frac{dp}{dx} - \frac{1}{B_T}\sum_{i=1}^{N-1} B_{y_i}\frac{dy_i}{dx} - \frac{U}{B_T}\frac{dU}{dx}. \quad (67)$$

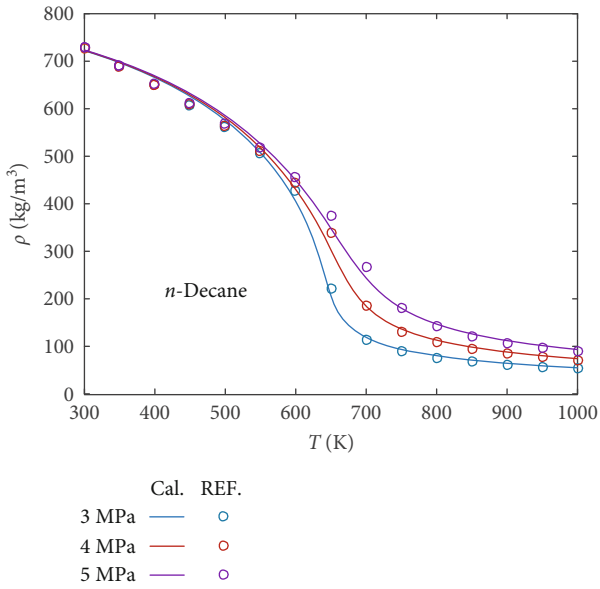

Figure 1: Comparison of densities of *n*-decane under different pressures.

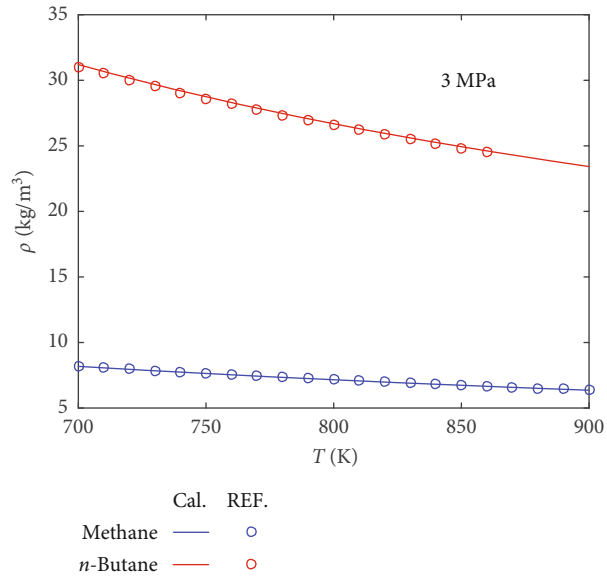

Figure 2: Comparison of densities of methane and *n*-butane under 3 MPa.

A two-step global reaction mechanism [36] based on the mechanism proposed by Ward et al. [37] is adopted to calculate the chemical production rates of species in the cooling channel in this study.

3.3. Equations for the Fuel Injector. It is assumed that fuel is isentropically accelerated to sonic speed in the fuel injector. By ignoring changes in fuel compositions, equations for the fuel injector are listed as follows:

$$h_o = h_{f,2} + \frac{1}{2}U_{f,2}^2 = h_{f,cr} + \frac{1}{2}a_{f,cr}^2, \tag{68}$$

$$s_{f,2} = s_{f,cr}, \tag{69}$$

$$\dot{m}_f = \rho_{f,2}U_{f,2}A_{c,2} = \rho_{f,cr}a_{f,cr}A_{cr}, \tag{70}$$

$$h_f = h\left(T_f, p_f\right), \tag{71}$$

$$\rho_f = \rho\left(T_f, p_f\right), \tag{72}$$

$$a_f = \sqrt{\frac{c_{pf}}{c_{vf}}\left(\frac{\partial p_f}{\partial \rho_f}\right)_{T,y_i}}, \tag{73}$$

where h_o is the total enthalpy of fuel, A_{cr} is the outlet area of fuel injector, and a_f is the sound speed of fuel. Because of the complexity of the RK-PR equation, the above equations need to be solved iteratively. Newton's iteration method is used in this study.

3.4. Calculation of the Wall Temperatures. Heat is transferred from the combustor wall to the cooling channel wall by heat conduction and then transferred to the fuel in the cooling channel by forced heat convection. The key to a heat convection problem is to calculate the convective heat transfer coefficient which relies on the heat transfer correlation. The heat transfer correlation of fuel in the cooling channel in this study [38] is shown in equation (74). The convective heat transfer coefficient can be calculated by equation (75).

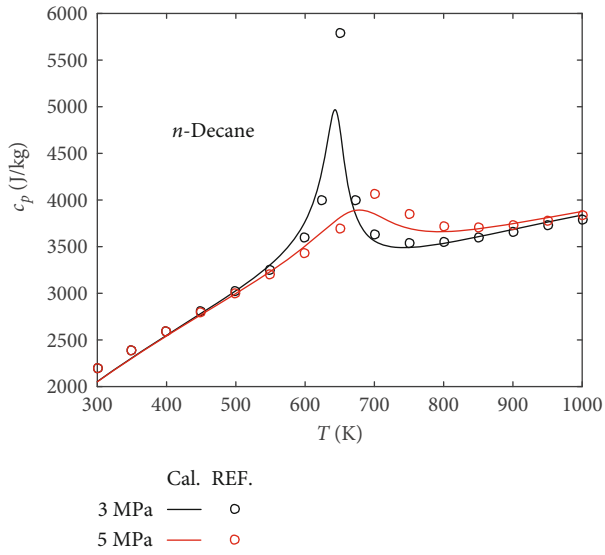

Figure 3: Comparison of constant-pressure specific heat capacities of *n*-decane under different pressures.

$$\mathrm{Nu}_f = 0.027\,\mathrm{Re}_f^{0.8}\mathrm{Pr}_f^{0.33}\left(\frac{\mu_f}{\mu_w}\right)^{0.14}, \tag{74}$$

$$h_c = \frac{\mathrm{Nu}_f\lambda_f}{D_r}, \tag{75}$$

where Nu_f, Re_f, and Pr_f are the Nusselt number, Reynolds number, and Prandtl number of fuel, respectively.

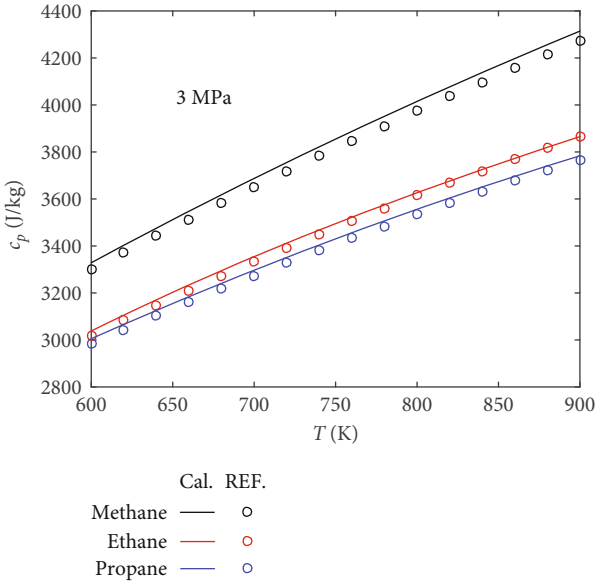

Figure 4: Comparison of constant-pressure specific heat capacities of methane, ethane, and propane under 3 MPa.

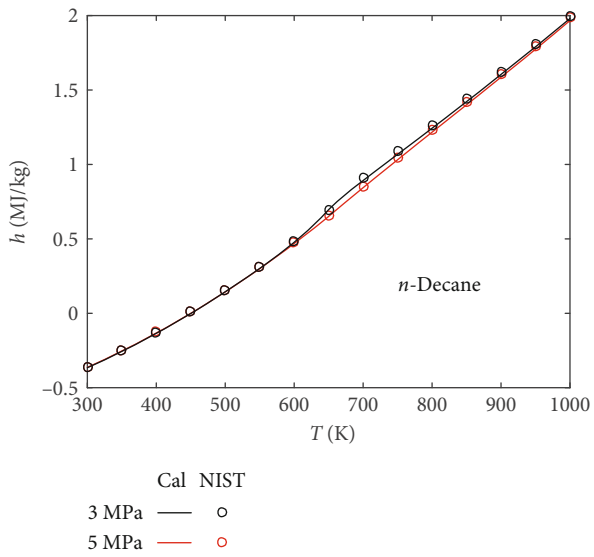

Figure 5: Comparison of enthalpies of n-decane under different pressures.

Variables μ_f and λ_f are viscosity and thermal conductivity of fuel, respectively, which can be calculated by the method proposed by Tong [39]. Variable μ_w is the viscosity of fuel adjacent to the cooling channel wall. Variable D_r is the hydraulic diameter of the cooling channel. After the wall temperature of cooling channel is obtained, wall temperature on the combustor side can be calculated by heat conduction through the combustor wall.

4. Solution Methodology

In the previous sections, different parts of a regeneratively cooled scramjet combustor are modeled separately. But in reality, these parts are coupled together physically. The coupling relationship of core variables between these parts was analyzed clearly by Zhang et al. [28]. The solution methodology proposed by Zhang et al. [28] is also adopted in this study.

Because of the time scales of chemical reactions, governing equations for the supersonic combustor and the cooling channel are stiff ordinary differential equations mathematically. The SUNDIALS code, a stiff ordinary differential equation solver developed by the Lawrence Livermore National Laboratory [40], is used to solve the governing equations in this study.

Figure 6: Comparison of enthalpies of methane, ethane, and propane under 3 MPa.

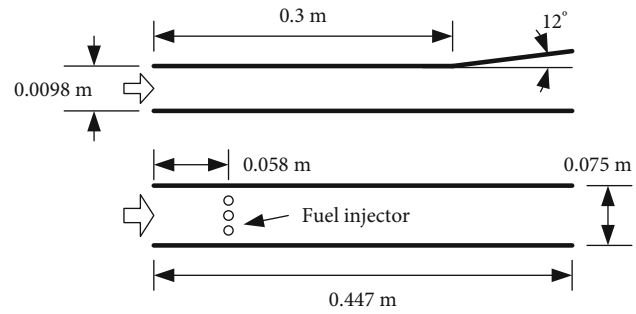

Figure 7: Geometry configuration of the HyShot II scramjet combustor.

5. Verification

5.1. Verification of the Thermodynamic Property Calculation Method. The thermodynamic property calculation method is verified by comparing the computational results with the data offered by REFPROP software which is provided by NIST (National Institute of Standards and Technology).

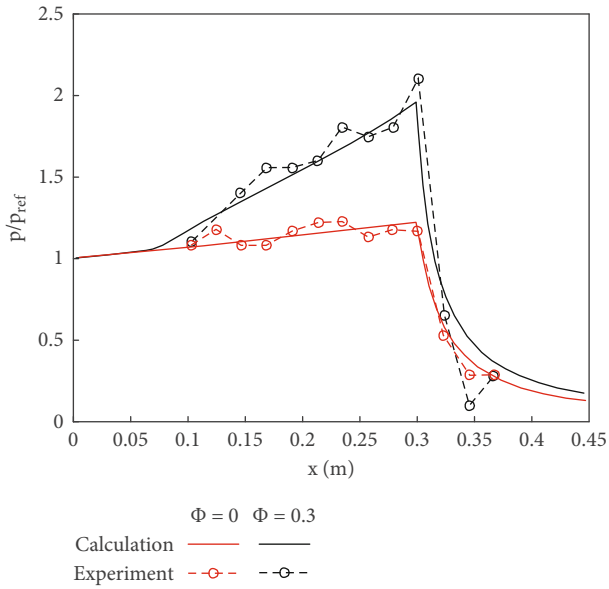

Figure 8: Comparison of computational results and experimental data of the HyShot II scramjet combustor.

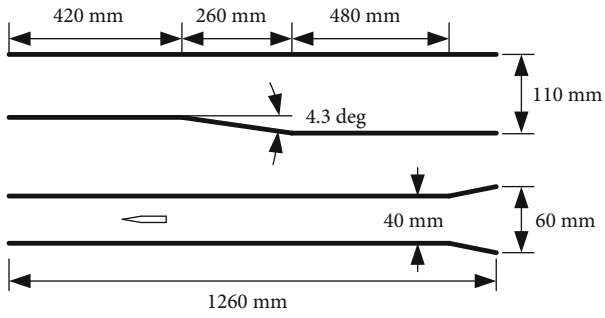

Figure 9: Geometry configuration of the supersonic combustor at HIT.

As shown in Figures 1–6, computation accuracies of thermodynamic properties such as density, enthalpy, and constant-pressure specific heat capacity are very high. Relatively large computational errors occur near the critical temperature of *n*-decane. However, this appears in a narrow temperature range. As a whole, the computational accuracies of the thermodynamic property calculation method are acceptable.

5.2. Verification of the Supersonic Combustor Model. The supersonic combustor model is verified by experimental results for both hydrogen and hydrocarbon-fueled scramjet combustors. The reason is that in a regeneratively cooled scramjet engine, fuel injected into the combustor is a mixture containing both small-molecule gases, such as hydrogen and methane, and long chain hydrocarbons.

Firstly, flight data of the HyShot II scramjet flight experiment [7] are adopted to verify the model. The combustor configuration is shown in Figure 7. Hydrogen is injected into the combustor at a location 58 mm from the combustor inlet. Conditions with fuel injection and without fuel injection are verified. A constant combustor wall temperature of 1200 K is assumed during the calculation. Figure 8 displays the computational results as well as the experimental data.

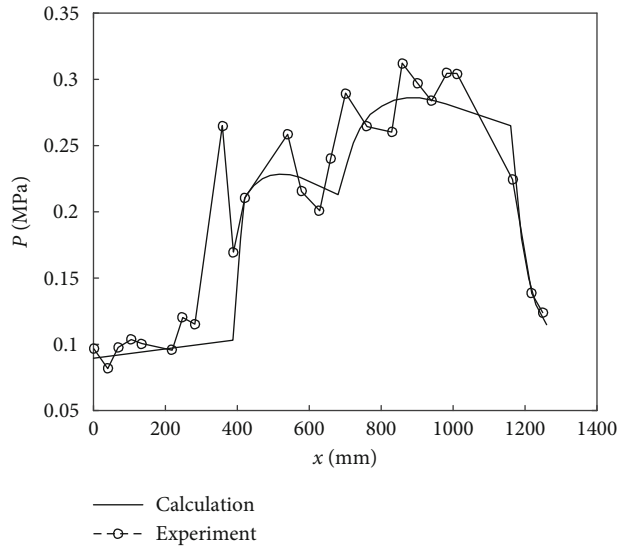

Figure 10: Comparison of computational results and experimental data obtained by the research group at HIT.

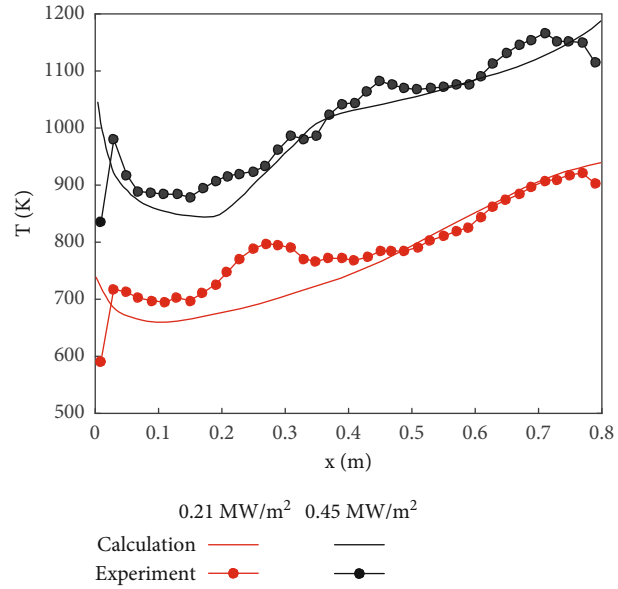

Figure 11: Comparison of computational and experimental results of cooling channel wall temperature.

Then, the model is verified by experimental results obtained by the research group of Professor Bao at Harbin Institute of Technology (HIT) [41]. The combustor configuration is shown in Figure 9. The scramjet combustor is kerosene-fueled and strut-injected. Experiments were taken at a direct-connected supersonic combustion test bench. The fuel equivalence ratio is 0.3. Computational results and experimental data are displayed in Figure 10.

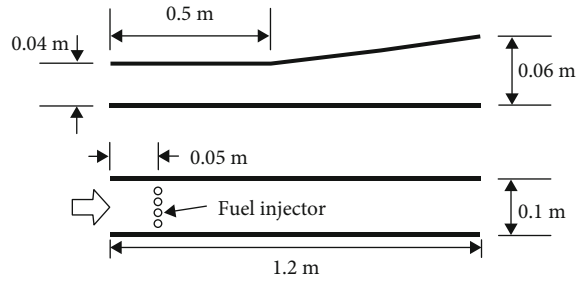

Figure 12: Geometry configuration of the supersonic combustor.

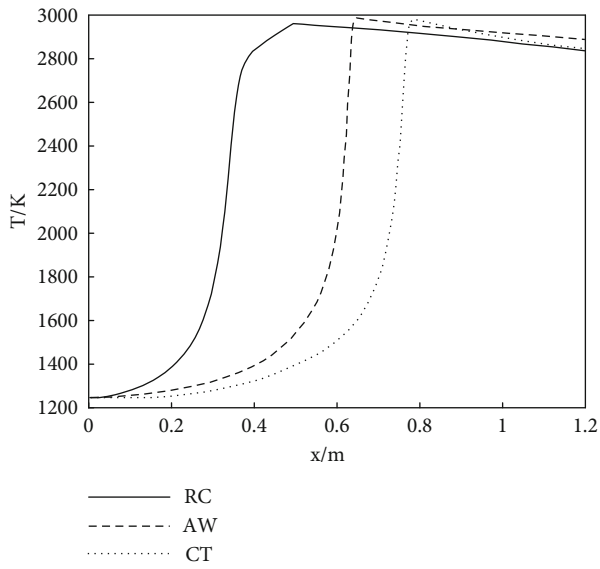

Figure 13: Temperature distributions along the combustor duct.

As shown in Figures 8 and 10, the model has a reasonable accuracy for both hydrogen and hydrocarbon-fueled scramjet combustors.

5.3. Verification of the Cooling Channel Model. Verification of the cooling channel model is accomplished by comparing the computational results with the experimental data reported in [42]. As reported in the literature, an electric heating tube test bench which could generate constant heat flux was built to conduct the experiments. *n*-Decane is used as a coolant. As shown in Figure 11, the computational results are in good agreement with the experimental data, which means that the cooling channel model has a reasonable accuracy.

6. Results and Discussion

The flow processes that happened in a regeneratively cooled scramjet combustor are really complex. Firstly, the flow processes that occurred in the supersonic combustor are complicated, which involve mass addition, supersonic mixing, chemical reaction, wall friction, heat transfer, etc. Secondly, the supersonic combustor is coupled with the cooling channel, which means that the flow processes happened in the supersonic combustor and the cooling channel interacts with each other. Finally, the fuel in the cooling channel will go through various processes, including supercritical flow and chemical reaction. So it is valuable to research the characteristics of a regeneratively cooled scramjet combustor.

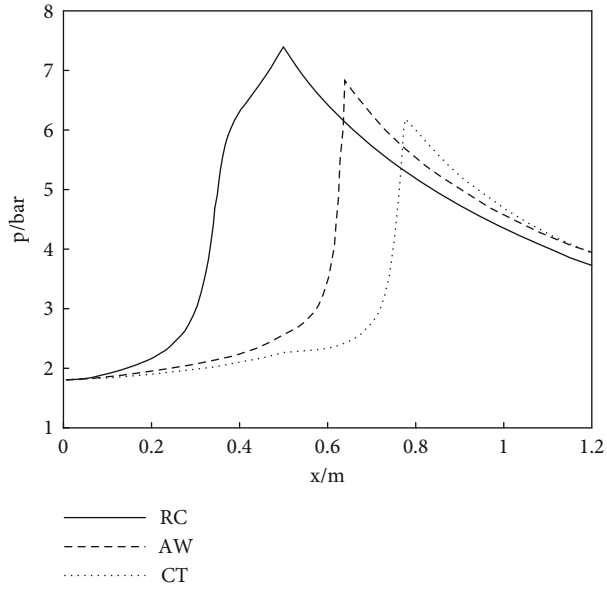

Figure 14: Pressure distributions along the combustor duct.

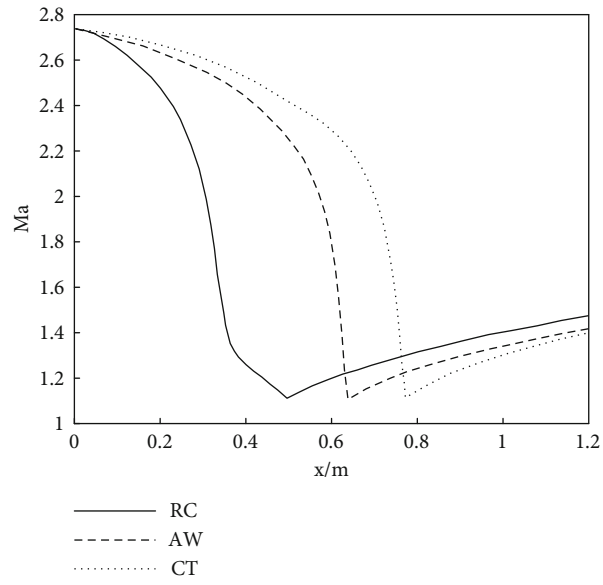

Figure 15: Mach number distributions along the combustor duct.

The geometry of the supersonic combustor is shown in Figure 12. The duct is composed of a constant cross-sectional area part followed by a diverging part. The sizes are clearly labeled in the figure. *n*-Decane is used as fuel instead of hydrogen. The fuel equivalence ratio is 1, and the fuel temperature is 280 K. The inlet conditions are the same as before. The characteristics of the supersonic

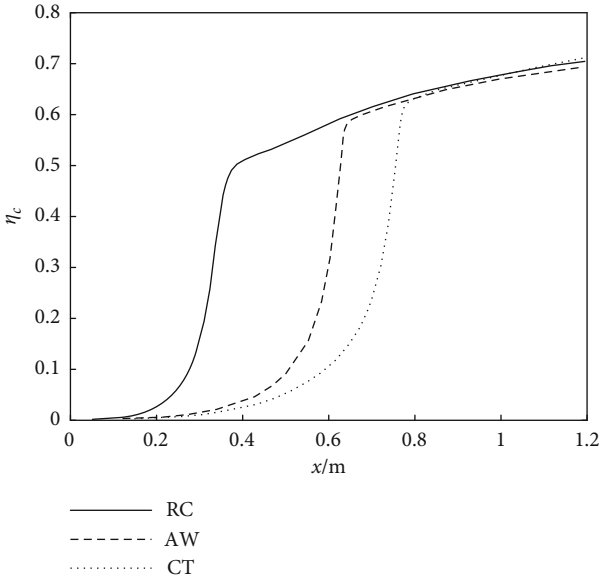

Figure 16: Combustion efficiency distributions along the combustor duct.

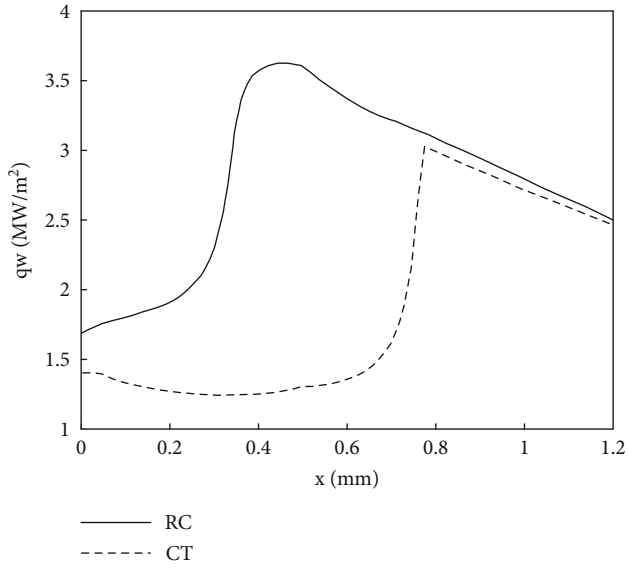

Figure 17: Distributions of wall heat flux along the cooling channel.

combustor are studied under three different boundary conditions: (1) the combustor wall with constant temperature of 1200 K, (2) the combustor with the adiabatic wall, and (3) the combustor with regenerative cooling. For simplicity, conditions 2 to 3 are referred to as CT, AW, and RC, respectively. In the case of CT, the heat transferred through the combustor wall is not recovered and dissipated to the surroundings. In the three cases, the mixing length is 1.5 m in the calculation of mixing efficiency.

The distributions of temperature, pressure, Mach number, and combustion efficiency along the combustor duct are displayed in Figures 13–16, respectively. Computational results of the three conditions are presented in each figure, where the combustion efficiency is defined as the ratio of the sum of mole friction of H_2O and CO_2 of real combustion products to that of ideal combustion products, as shown in

$$\eta_C = \frac{x_{H_2O} + x_{CO_2}}{\left[x_{H_2O} + x_{CO_2}\right]_{\text{ideal}}}. \quad (76)$$

As shown in the figures, the ignition delay time in RC is the shortest among the three conditions. The ignition happens in the constant cross-sectional area part of the combustor. This is because the temperature and species of fuel change dramatically owing to the regenerative cooling process. High temperature and small molecule gases are beneficial to the ignition process. For the other two conditions under which the cold fuel is directly injected into the combustor, the ignition occurs in the diverging part of the combustor. In CT, because of heat dissipation, the ignition delay time and the ignition distance are the longest, which results in the lowest peak pressure compared to other two conditions.

From the viewpoint of energy conservation, energy is conserved in RC and AW, but dissipated in CT, which can be reflected by the temperature and Mach number of the

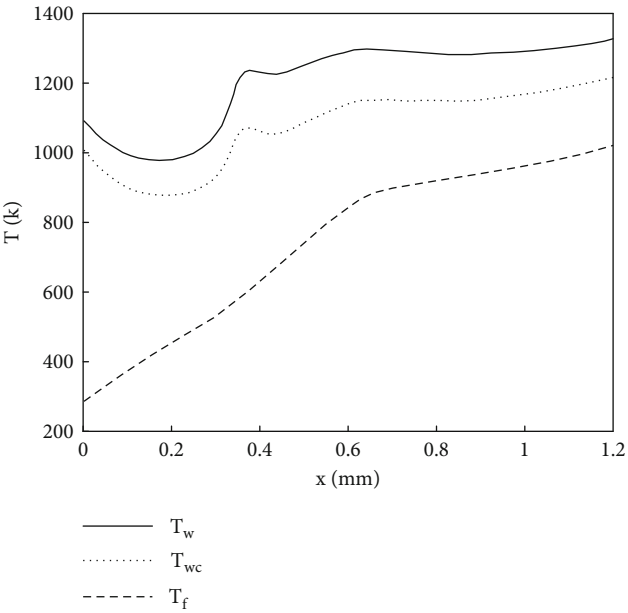

Figure 18: Distributions of wall temperature and fuel temperature.

combustor outlet. In CT, the temperature and Mach number of the combustor outlet are the lowest, which results from the dissipation of energy. In RC, the temperature of the combustor outlet is lower than the one in AW. However, the Mach number of the combustor outlet is higher than the one in AW. This means that more thermal energy of gases is converted into kinetic energy in RC, which is one of the advantages of regenerative cooling.

Combustion efficiencies at the combustor outlet under the three conditions are nearly the same, which is about 70%. Due to the different ignition delay time, the combustion efficiency distributions along the combustor duct are different.

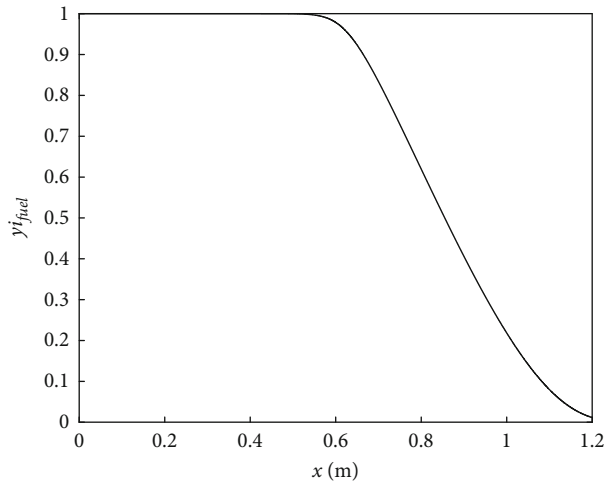

Figure 19: Distributions of fuel mass fraction along the cooling channel.

The distributions of wall heat flux are displayed in Figure 17. As shown in the figure, wall heat flux in RC is much higher than the one in CT, which is one of the features of regeneratively cooled scramjets. Owing to the regenerative cooling, the wall temperature in RC is lower than the one in CT which results in a higher wall heat flux. The distributions of wall temperature and fuel temperature are presented in Figure 18. At the inlet of the cooling channel, the wall temperature is significantly below the limit temperature of the material because of the regenerative cooling. With fuel flowing through the cooling channel, the fuel temperature and the wall temperature increase gradually until the material was burned up or the coke of fuel formed. The distributions of mass fraction of fuel along the cooling channel are displayed in Figure 19. With the fuel temperature increasing, the thermal cracking reactions gradually occur and the mass fraction of fuel gradually decreases.

7. Conclusion

A quasi-one-dimensional model of hydrocarbon-fueled scramjet combustors coupled with regenerative cooling has been developed to analyze the characteristics of the regeneratively cooled scramjet combustors. The model is composed of a supersonic combustor model with finite-rate chemistry and a cooling channel model with real gas working medium. By applying appropriate solution methodology, flow variables of the supersonic combustor and cooling channel can be calculated, based on which the characteristics of the regeneratively cooled scramjet combustor are studied. Examples of hydrocarbon-fueled scramjets with strut injectors were taken under the flight Mach number of 8 at 30 km. Three cases were comparatively studied: (1) scramjet combustor with the isothermal wall, (2) scramjet combustor with the adiabatic wall, and (3) scramjet combustor with regenerative cooling. The ignition delay time of the scramjet combustor with regenerative cooling is the shortest because the small molecule products have lower activation energy. Compared with the scramjet combustor with the isothermal wall, heat flux of the scramjet combustor with regenerative cooling increases significantly. This new model can give a relatively reasonable description of the flow phenomenon involved in the hydrocarbon-fueled regeneratively cooled scramjet engine. Further work such as optimization of engine configuration and performance will be continued based on it.

Nomenclature

A: area (m^2)
a: Sound speed (m/s)
C_f: Wall friction coefficient
c_p: constant pressure specific heat (J/kg/K)
c_v: constant volume specific heat (J/kg/K)
D: Hydraulic diameter (m)
e: Specific internal energy (J/kg)
f: Drag coefficient
h: Specific enthalpy (J/kg)
h_c: Convective heat transfer coefficient
h_o: Total specific enthalpy (J/kg)
L_{mix}: Mixing length (m)
Ma: Mach number
M_w: Molar mass (kg/mol)
$\overline{M_w}$: Mean molar mass (kg/mol)
$\dot{m}$: Mass flow rate (kg/s)
Nu: Nusselt number
P: Pressure (Pa)
Pr: Prandtl number
P_w: Perimeter (m)
q_w: Density of heat flux (W/m^2)
Re: Reynolds number
R_u: Universal gas constant (J/mol/K)
s: Specific entropy (J/kg/K)
T: Temperature (K)
U: Velocity (m/s)
x: Location along the duct (m)
y: Mass fraction
Φ_c: Heat flow through the wall (W)
γ: Specific heat ratio
ε: The ratio of velocity in x direction to velocity magnitude
η_m: Mixing efficiency
θ: Thickness of the combustor wall (m)
λ: Thermal conductivity (W/m/K)
μ: Viscosity (Pa/s)
ρ: Density (kg/m^3)
$\dot{\omega}$: Molar production rate ($mol/m^3/s$).

Subscripts

0: Evaluated at 1 atm
c: Cooling channel
comb: Combustor
f: Fluid in the cooling channel
i: Species i
m: Mixture
w: Wall condition on the combustor side

wc: Wall condition on the cooling side.

Superscripts

∗: Evaluated at reference temperature.

Data Availability

The experimental data used to support the findings of this study are included within the article.

Conflicts of Interest

The authors declare that they have no conflicts of interest.

Acknowledgments

This research was supported by Programs of the National Natural Science Foundation of China (No. 52076051).

References

[1] E. T. Curran, "Scramjet engines: the first forty years," *Journal of Propulsion and Power*, vol. 17, no. 6, pp. 1138–1148, 2001.

[2] R. J. Stalker, A. Paull, D. J. Mee, R. G. Morgan, and P. A. Jacobs, "Scramjets and shock tunnels–the Queensland experience," *Progress in Aerospace Sciences*, vol. 41, no. 6, pp. 471–513, 2005.

[3] Z. Dong, D. Li, Z. Wang, and M. Sun, "A review on exergy analysis of aerospace power systems," *Acta Astronautica*, vol. 152, pp. 486–495, 2018.

[4] W. Heiser and D. Pratt, *Hypersonic Airbreathing Propulsion*, AIAA, Washington, D.C., 1994.

[5] R. Daines and C. Segal, "Combined rocket and airbreathing propulsion systems for space-launch applications," *Journal of Propulsion and Power*, vol. 14, no. 5, pp. 605–612, 1998.

[6] M. Chen, H. Tang, K. Zhang, O. Hui, and Y. Wang, "Turbine-based combined cycle propulsion system integration concept design," *Proceedings of the Institution of Mechanical Engineers, Part G: Journal of Aerospace Engineering*, vol. 227, no. 7, pp. 1068–1089, 2013.

[7] M. K. Smart, N. E. Hass, and A. Paull, "Flight data analysis of the HyShot 2 scramjet flight experiment," *AIAA Journal*, vol. 44, no. 10, pp. 2366–2375, 2006.

[8] P. L. Moses, V. L. Rausch, L. T. Nguyen, and J. R. Hill, "NASA hypersonic flight demonstrators–overview, status, and future plans," *Acta Astronautica*, vol. 55, no. 3-9, pp. 619–630, 2004.

[9] Y. Tsujikawa, Y. Tsukamoto, and S. Fujii, "Performance analysis of scramjet engine with quasi-one-dimensional flow model," *Ternational Journal of Hydrogen Energy*, vol. 16, no. 2, pp. 135–142, 1991.

[10] T. F. O'Brien, R. P. Starkey, and M. J. Lewis, "Quasi-one-dimensional high-speed engine model with finite-rate chemistry," *Journal of Propulsion and Power*, vol. 17, no. 6, pp. 1366–1374, 2001.

[11] M. R. Tetlow and C. J. Doolan, "Comparison of hydrogen and hydrocarbon-fueled scramjet engines for orbital insertion," *Journal of Spacecraft and Rockets*, vol. 44, no. 2, pp. 365–373, 2007.

[12] S. Tomioka, T. Hiraiwa, K. Kobayashi, M. Izumikawa, T. Kishida, and H. Yamasaki, "Vitiation effects on scramjet engine performance in Mach 6 flight conditions," *Journal of Propulsion and Power*, vol. 23, no. 4, pp. 789–796, 2007.

[13] C. Birzer and C. J. Doolan, "Quasi-one-dimensional model of hydrogen-fueled scramjet combustors," *Journal of Propulsion and Power*, vol. 25, no. 6, pp. 1220–1225, 2009.

[14] S. H. Kang, Y. J. Lee, S. S. Yang, and B. Choi, "Effects of flameholder configurations on combustion in scramjet engines," *Journal of Propulsion and Power*, vol. 28, no. 4, pp. 739–746, 2012.

[15] J. Noda, A. Murakami, K. Kudo, and S. Tomioka, "Estimation of mode transition in a supersonic combustor," *Journal of Thermal Science and Technology*, vol. 8, no. 2, pp. 353–362, 2013.

[16] W. Bao, Y. J. Duan, W. X. Zhou, and D. Yu, "Hydrogen-fueled scramjet cooling system investigation using combustor and regenerative cooling coupled model," *Proceedings of the Institution of Mechanical Engineers, Part G: Journal of Aerospace Engineering*, vol. 228, no. 6, pp. 820–830, 2014.

[17] L. Tian, L. Chen, Q. Chen, F. Li, and X. Chang, "Quasi-one-dimensional multimodes analysis for dual-mode scramjet," *Journal of Propulsion and Power*, vol. 30, no. 6, pp. 1559–1567, 2014.

[18] L. Tian, L. H. Chen, Q. Chen, F. Q. Zhong, and X. Y. Chang, "Engine performance analysis and optimization of a dual-mode scramjet with varied inlet conditions," *Acta Mechanica Sinica*, vol. 32, no. 1, pp. 75–82, 2016.

[19] A. Goel, A. Xie, K. Duraisamy, and D. S. Bernstein, "Retrospective cost adaptive thrust control of a 1D scramjet with Mach number disturbance," *Proceeding of the American Control Conference*, pp. 5551–5556, 2015.

[20] L. Wang, S. Li, H. Chi, B. Li, Z. Wei, and N. Wang, "Quasi-one-dimensional numerical method for solid fuel scramjet combustor analysis and design," *Journal of Aerospace Engineering*, vol. 28, no. 3, 2015.

[21] M. K. Smart, "Flow modeling of pseudoshocks in backpressured ducts," *AIAA Journal*, vol. 53, no. 12, pp. 3577–3588, 2015.

[22] T. Vanyai, M. Bricalli, S. Brieschenk, and R. R. Boyce, "Scramjet performance for ideal combustion processes," *Aerospace Science and Technology*, vol. 75, pp. 215–226, 2018.

[23] K. Cheng, Y. Feng, Y. Jiang et al., "Thermodynamic analysis for recuperation in a scramjet nozzle with wall cooling," *Applied Thermal Engineering*, vol. 121, pp. 153–162, 2017.

[24] J. A. Schetz, F. S. Billig, and S. Favin, "Analysis of slot injection in hypersonic flow," *Journal of Propulsion and Power*, vol. 7, no. 1, pp. 115–122, 1991.

[25] T. Kanda, G. Masuya, F. Ono, and Y. Wakamatsu, "Effect of film cooling/regenerative cooling on scramjet engine performances," *Journal of Propulsion and Power*, vol. 10, no. 5, pp. 618–624, 1994.

[26] J. Y. Zuo, S. L. Zhang, J. Qin, W. Bao, and N. G. Cui, "Performance evaluation of regenerative cooling/film cooling for hydrocarbon fueled scramjet engine," *Acta Astronautica*, vol. 148, pp. 57–68, 2018.

[27] F. Chen, W. Tam, N. Shimp, and R. Norris, "An innovative thermal management system for a Mach 4 to Mach 8 hypersonic scramjet engine," in *In 34th AIAA/ASME/SAE/ASEE joint propulsion conference and exhibit*, p. 3734, Cleveland, OH, U.S.A., 1998.

[28] D. Zhang, Y. Feng, S. L. Zhang et al., "Quasi-one-dimensional model of scramjet combustor coupled with regenerative

cooling," *Journal of Propulsion and Power*, vol. 32, no. 3, pp. 687–697, 2016.

[29] C. R. McClinton, V. L. Rausch, L. T. Nguyen, and J. R. Sitz, "Preliminary X-43 flight test results," *Acta Astronautica*, vol. 57, no. 2-8, pp. 266–276, 2005.

[30] Y. V. Khankhasaeva, V. E. Borisov, and A. E. Lutsky, "Influence of energy input on the flow past hypersonic aircraft X-43," *Journal of Physics Conference Series*, vol. 815, p. 012018, 2017.

[31] J. M. Hank, J. S. Murphy, and R. C. Mutzman, "The X-51A scramjet engine flight demonstration program," *AIAA Paper*, p. 2540, 2008.

[32] K. Kundu, P. Penko, and S. Yang, "Reduced reaction mechanisms for numerical calculations in combustion of hydrocarbon fuels," in *In 36th AIAA Aerospace Sciences Meeting and Exhibit*, p. 803, Reno, NV, U.S.A., 1998, January.

[33] S. K. Kim, H. S. Choi, and Y. Kim, "Thermodynamic modeling based on a generalized cubic equation of state for kerosene/LOx rocket combustion," *Combustion and Flame*, vol. 159, no. 3, pp. 1351–1365, 2012.

[34] M. Cismondi and J. Mollerup, "Development and application of a three-parameter RK-PR equation of state," *Fluid Phase Equilibria*, vol. 232, no. 1-2, pp. 74–89, 2005.

[35] H. Meng and V. Yang, "A unified treatment of general fluid thermodynamics and its application to a preconditioning scheme," *Journal of Computational Physics*, vol. 189, no. 1, pp. 277–304, 2003.

[36] H. W. Li, *Research on Characteristics of the High Temperature Gaseous Hydrocarbon Fuel Expansion Power Generation System for Hypersonic Propulsion*, Harbin Institute of Technology, Harbin, Heilongjiang, 2019.

[37] T. A. Ward, J. S. Ervin, R. C. Striebich, and S. Zabarnick, "Simulations of flowing mildly-cracked normal alkanes incorporating proportional product distributions," *Journal of Propulsion and Power*, vol. 20, no. 3, pp. 394–402, 2004.

[38] Y. J. Duan, *Optimization Investigation of Active Thermal Protection Structure and Performance for Scramjet Engines, Ph. D. Dissertation*, School of Energy Science and Engineering, Harbin Institute of Technology, Harbin, Heilongjiang, 2012.

[39] J. S. Tong, "Fluid thermophysical properties," *Beijing*, pp. 198–203, 2008.

[40] A. C. Hindmarsh, P. N. Brown, K. E. Grant et al., "SUNDIALS," *ACM Transactions on Mathematical Software*, vol. 31, no. 3, pp. 363–396, 2005.

[41] Q. Yang, J. Chang, and W. Bao, "Relative time scale analysis for pressure propagation during ignition process of a scramjet," *Aerospace Science and Technology*, vol. 39, pp. 206–210, 2014.

[42] D. Zhang, *Investigation of Power Generation System Driven by Fuel Vapor Turbine on a Hydrocarbon Scramjet, Ph. D. Dissertation*, School of Energy Science and Engineering, Harbin Institute of Technology, Harbin, Heilongjiang, 2016.